MMTO Technical Memorandum #03-2

Smithsonian Institution &
The University of Arizona®

Test Report for MMT F/5 Secondary Mirror

Steward Observatory Mirror Lab

January 2003

Test report for MMT f/5 secondary mirror

Buddy Martin

January 21, 2003

1. Summary

We present results of measuring the MMT f/5 secondary mirror, and encircled energy calculations derived from the figure measurements. The mirror has an rms surface error of 17 nm when astigmatism and spherical aberration are subtracted (about 34 nm rms uncorrected). When combined with the MMT primary, the secondary increases the 80%-encircled-energy diameter from 0.14″ to 0.20″ in perfect seeing, and from 0.54″ to 0.56″ in 0.25″ seeing. The MMT primary and a secondary whose structure function matches the target give 80% diameters of 0.17″ in perfect seeing and 0.55″ in 0.25″ seeing.

Figure measurements have been hampered by problems with the holographic Fizeau test system. These problems cause a loss of some data near the edge of the mirror, and distortion of the image.

The radius of curvature and conic constant fall in the tolerance window.

2. Measurement system

The measurement is made with a holographic test plate as shown in Figure 1. The test system was designed by Jim Burge and assembled by Lee Dettmann. It is described in detail in Reference 1 and briefly described here. Interference fringes are formed between a wavefront reflected by the secondary mirror and a wavefront diffracted by a computer-generated hologram on the surface of the test plate. These surfaces are separated nominally by 5 mm. The hologram is designed to diffract a wavefront that matches that reflected by a perfect secondary mirror. The rest of the test system serves to illuminate the secondary and hologram with light that is normal to the surfaces within about 1 mrad. Errors in the illumination system are common to both interfering wavefronts and therefore cancel to first order. The quality of the illumination system was specified to make higher order effects negligible.

The two types of errors that directly affect the measurement are the shape of the test plate surface and the positions of the hologram's rings. Based on extensive tests, we trust the hologram writer to place the rings accurately to about 1 micron rms in radius, adequate to reduce the resulting wavefront error to 5 nm rms. We measure the spherical surface of the test plate directly with an interferometer from its center of curvature. This measurement is made immediately before or after each measurement of the secondary. The test plate has significant errors, >100 nm rms surface, so they must be measured and subtracted accurately.

The measurement of the secondary and that of the test plate are made with two different imaging systems, so we must transform the images into a common coordinate system in order to subtract the test plate figure from the measured secondary figure. This was done initially by placing 4 fiducial markers (bits of paper) at known locations on the secondary and the test plate, and measuring their location in each image. The commercial measurement system performs linear transformations (displacement, magnification, flip, rotation, aspect ratio and shear) to obtain the best fit to the fiducial locations, thereby putting each image into physical coordinates. The system can also perform limited non-linear mapping (correction of distortion).

We found that the image of the secondary seen through the illumination system and test plate has severe distortion, including abrupt changes in mapping near the edge of the mirror. We do not understand the cause of this distortion but believe it is related to slope errors in the 2.5 m illumination reflector. This

distortion causes errors in registration of the surfaces to be subtracted, and hence leaves errors in the difference. We measured the distortion using a mask with 400 holes over the mirror and found residual distortion >25 mm at some locations, leading to maximum measurement errors of about 100 nm surface. We have not succeeded in reducing these errors to an acceptable level and have therefore eliminated data where the distortion is greatest.

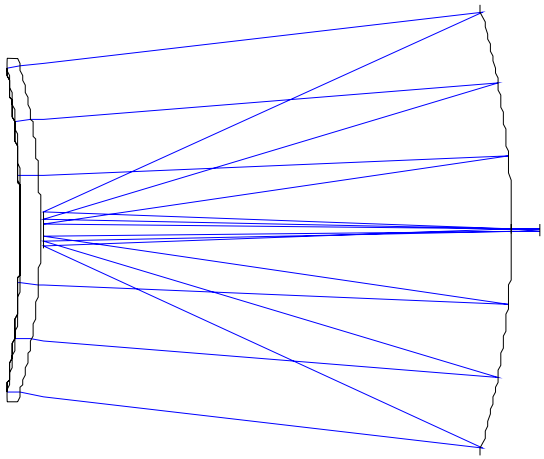

Figure 1. Test configuration for the f/5 secondary. The secondary mirror, not shown, would be at left. The 1.8 m holographic test plate, shown at left, is spaced 5 mm (nominal gap) from the secondary. The 2.5 m illumination primary mirror is at right and a small illumination secondary is attached to the center of the test plate. Source and camera are at far right.

We found that one quadrant of the image had less distortion than the rest, probably because the corresponding part of the illuminator has smaller slope errors. For the final measurements we rotated the secondary mirror through the best part of the illuminator in roughly 60° increments. Each map covers most of the aperture but has distortion greater than 25 mm in some small regions. We eliminated these regions—which would have inaccurate subtraction of the test plate's figure—from each map, transformed all maps to common mirror-based coordinates, overlaid the maps, and averaged the surface error in the overlapping regions. This stitching, performed with Lee Dettmann's Phase Mosaic program, adjusts all alignment aberrations (piston, tip, tilt, focus, and coma) of the individual maps to give the best match in the overlap region. The maps are overlaid based on approximately 100 fiducial markers obtained from the 400-hole mask (i. e., every other hole in each dimension).

3. Figure measurements

Figure measurements were made by Bryan Smith and Lee Dettmann. Figure 2 is a map of the surface error obtained by stitching the six individual maps made with the mirror at different rotation angles. The rms surface error over the clear aperture is 34 nm. Figure 3 shows the result of subtracting astigmatism and spherical aberration. The rms surface error is 17 nm.

The encircled energy diagrams are based on the map with astigmatism and spherical subtracted. Astigmatism will probably change significantly when the mirror is installed in the telescope support, and can be removed by adjusting the primary mirror. (This compensation is valid over the entire field of view.) Residual spherical aberration is included as an error in conic constant rather than a wavefront error.

Figure 4 shows the square root of the wavefront structure function, i. e. the rms wavefront difference between points in the aperture as a function of their separation. The structure function in Figure 4 is evaluated over the clear aperture for spectroscopy, D = 1.688 m. The target structure function corresponds to 0.022″ seeing and 1.5% scattering loss at 500 nm. The measured structure function exceeds the target values for separations less than about 20 cm on the secondary (about 80 cm on the primary). Figure 5 shows the same quantity evaluated over the clear aperture for imaging, D = 1.636 m.

Figure 6 shows the encircled energy for the MMT f/5 system in perfect seeing, including all combinations of perfect and actual primary and secondary mirrors. Compared with the primary alone, the secondary increases the 80% energy diameter from 0.14″ to 0.20″. Figure 7 shows the encircled energy in 0.25″ seeing. The secondary increases the 80% diameter from 0.54″ to 0.56″. Figure 8 and Figure 9 show the encircled energy for a combination of the actual primary and a secondary whose structure function matches the target. The 80% diameter is 0.17″ in perfect seeing and 0.55″ in 0.25″ seeing.

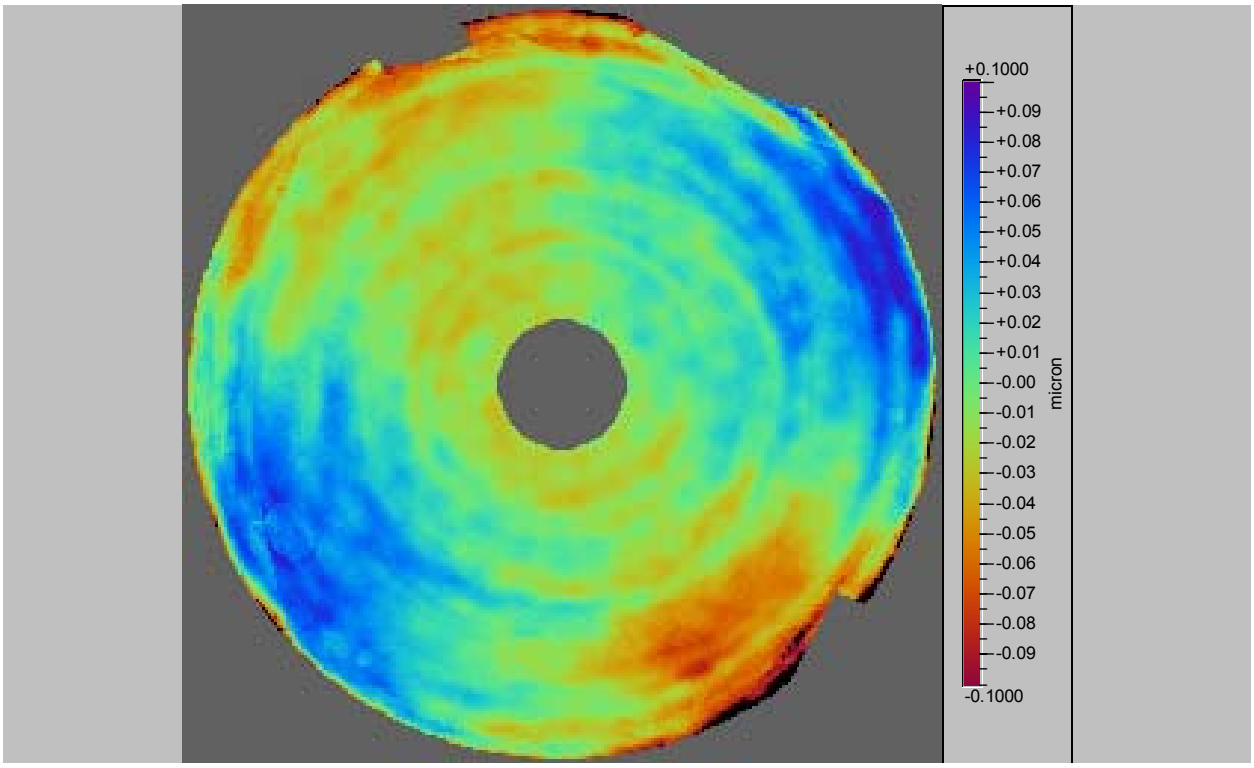

Figure 2. Map of surface error, obtained by stitching 6 individual maps with the mirror at different orientations. 34 nm rms surface error. Map is trimmed to clear aperture diameter *D* = 1.688 m.

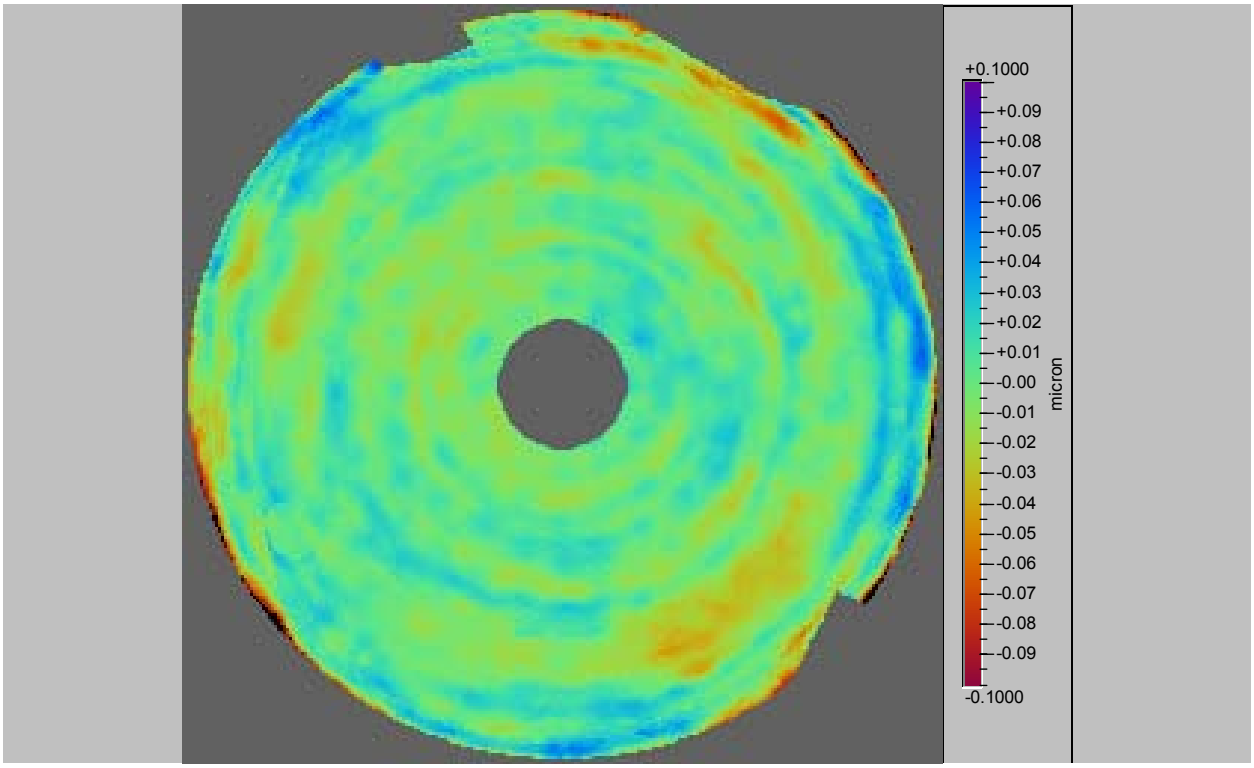

Figure 3. Same as Figure 2 but with astigmatism and spherical aberration subtracted. 17 nm rms surface error.

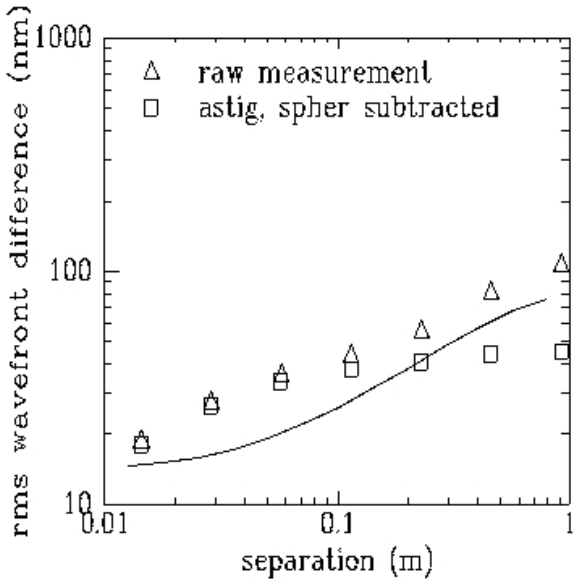

Figure 4. Structure function for maps with and without subtraction of astigmatism and spherical, evaluated over the clear aperture for spectroscopy, *D* = 1.688 m. The curve is the target, corresponding to 0.022″ seeing and 1.5% scattering loss at 500 nm.

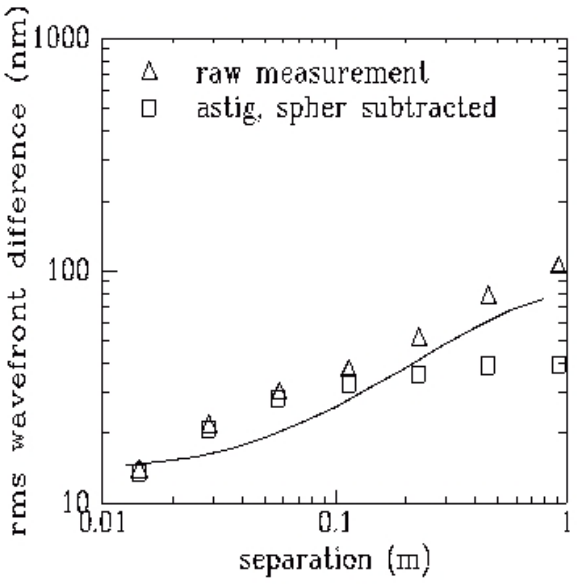

Figure 5. Same as Figure 4 but evaluated over the clear aperture for imaging, *D* = 1.636 m.

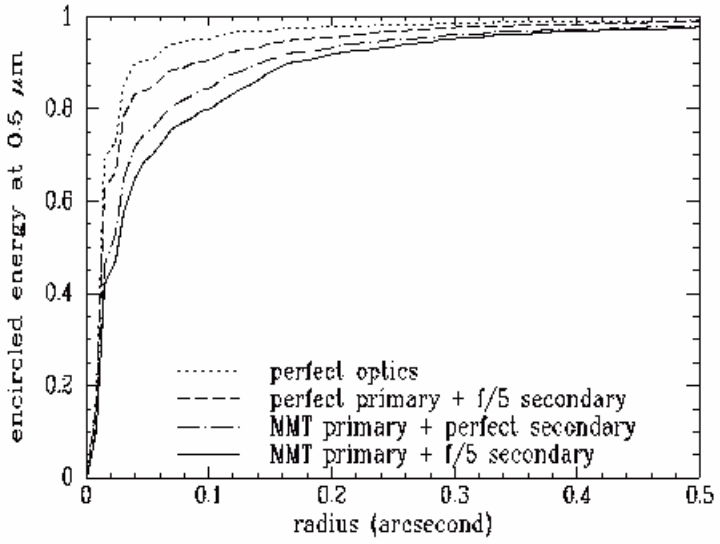

Figure 6. Encircled energy for MMT f/5 system in perfect seeing. Curves are shown for all combinations of perfect mirrors and measured mirror figures.

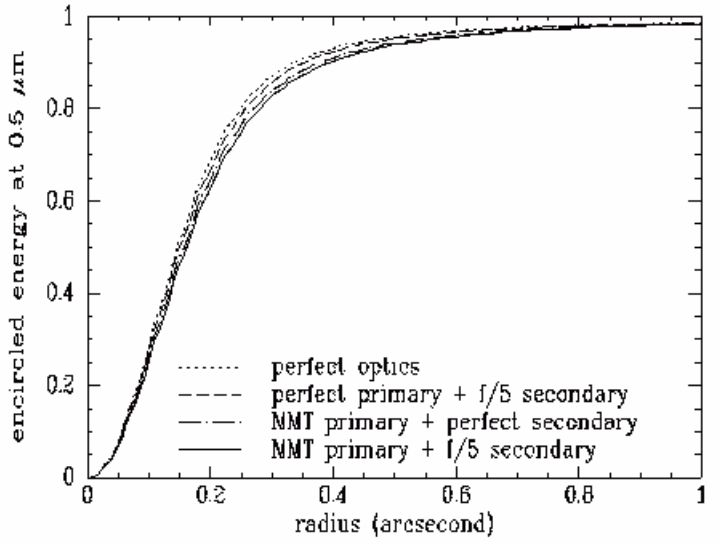

Figure 7. Encircled energy for MMT f/5 system in 0.25″ seeing. Curves are shown for all combinations of perfect mirrors and measured mirror figures.

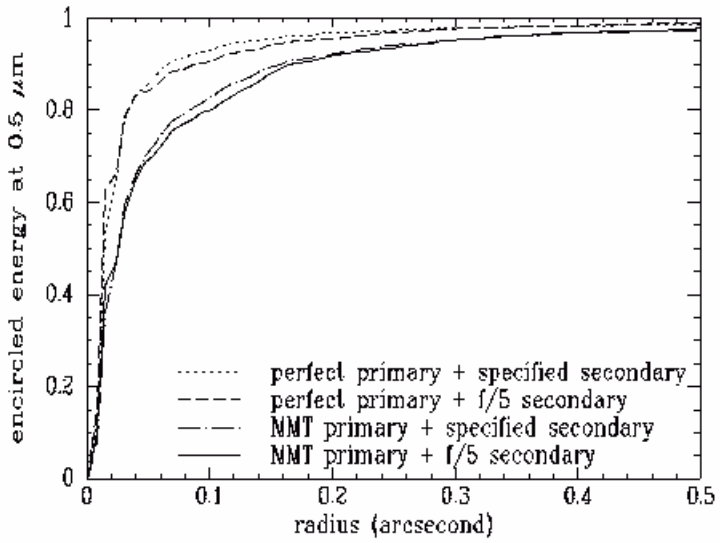

Figure 8. Encircled energy for MMT f/5 system in perfect seeing. Curves are shown for a perfect primary and the actual primary, and for the specified secondary and the actual secondary.

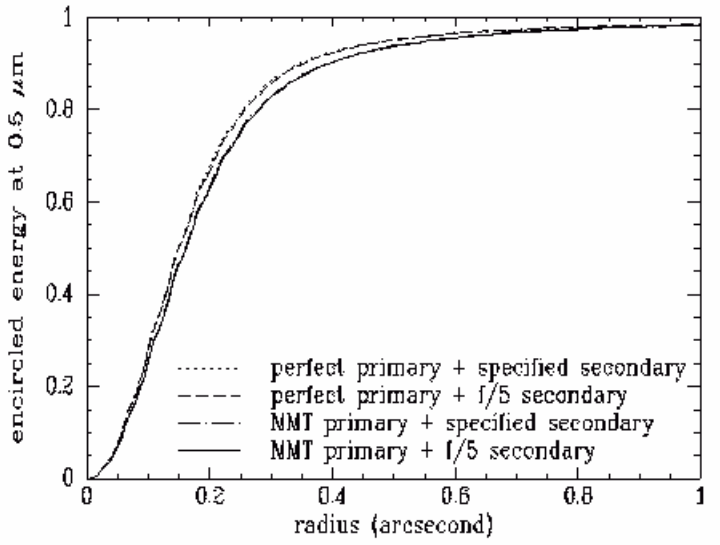

Figure 9. Encircled energy for MMT f/5 system in 0.25″ seeing. Curves are shown for a perfect primary and the actual primary, and for the specified secondary and the actual secondary.

4. Radius and conic constant

The prescribed mirror surface is a hyperboloid given in cylindrical polar coordinates (r,z) by

$$z = \frac{r^2}{R\left(1+\sqrt{1-(k+1)\frac{r^2}{R^2}}\right)}, \tag{1}$$

where the vertex radius of curvature and conic constant are

$$R = -5151.32 \text{ mm}, \tag{2}$$

$$k = -2.6946. \tag{3}$$

The specification includes a coupled tolerance on R and k. The relation is

$$\Delta k = 0.00047\left(\frac{\Delta R}{1 \text{ mm}}\right) \pm 0.001. \tag{4}$$

The measurements of radius of curvature and conic constant depend on the test plate and its hologram. The hologram is designed so that its diffracted wavefront matches the wavefront reflected by a secondary mirror with the nominal radius and conic constant, and at a particular distance (5 mm) from the test plate. More generally, the diffracted wavefront matches the wavefront reflected by a *family* of secondary mirrors with radius of curvature and conic constant depending on the distance, or gap, between test plate and secondary mirror. All members of this family produce reflected wavefronts that are identical at the surface of the test plate, and therefore give the same null interference pattern. We distinguish which member of the family our secondary is by measuring the gap. The relation between radius, conic constant, and gap t is

$$\delta R = \delta t, \tag{5}$$

$$\frac{\delta k}{k} = -\frac{\delta t}{R}, \tag{6}$$

where δ refers to departures from the nominal values.[2]

The inferred radius of curvature R also depends on the radius of curvature of the test plate. The test plate's radius was measured before the hologram was written, giving a value

$$R_{TP} = 5390.40 \text{ mm}, \tag{7}$$

and the hologram was designed to match it. (R_{TP} is defined as positive.) A subsequent measurement showed a roughly half-mm error in R_{TP}. This affects both the radius of curvature and the conic constant of the secondary mirror. The relationship is[2]

$$\delta R = -\delta R_{TP}, \tag{8}$$

$$\frac{\delta k}{k} = 3\frac{\delta R_{TP}}{R_{TP}}. \tag{9}$$

An additional correction to k must be made for spherical aberration in the final figure. If the surface spherical aberration is written as $S(6\rho^4 - 6\rho^2 + 1)$, where ρ is the polar coordinate normalized to 1 at the edge of the clear aperture, the error in conic constant is

$$\delta k = \frac{768 S R^3}{D^4}, \tag{10}$$

where the clear aperture diameter $D = 1.688$ m.

The measured and inferred values are listed in Table 1. The radius of curvature and conic constant fall well inside the tolerance window. The quoted uncertainties are 1-σ values.

Table 1. Measurement of radius of curvature and conic constant

parameter	value	uncertainty
Test parameters:		
nominal radius of test plate	5394.40 mm	
measured radius of test plate	5394.92 mm	0.20 mm
error in radius of test plate	0.52 mm	0.20 mm
nominal gap	5.00 mm	
measured gap	5.95 mm	0.05 mm
error in gap	0.95 mm	0.05 mm
Secondary mirror parameters:		
nominal radius of curvature	-5151.32 mm	
radius error due to test plate radius	-0.52 mm	0.20 mm
radius error due to gap	0.95 mm	0.05 mm
departure from nominal radius	0.43 mm	0.21 mm
actual radius of curvature	-5150.89 mm	0.21 mm
nominal conic constant	-2.6946	
desired change in conic constant for actual radius of curvature	0.0002	0.0001
desired conic constant based on actual radius of curvature	-2.6944	0.0001
measured spherical aberration	-90 nm	20 nm
conic error due to spherical	0.0012	0.0003
conic error due to test plate radius	-0.0008	0.0003
conic error due to gap	-0.0005	0.0000
departure from nominal conic	-0.0001	0.0004
actual conic constant	-2.6947	0.0004

5. Location of optical axis

The optical axis is located by aligning the secondary optically to the test plate (eliminating tilt and coma), and measuring the decenter of the test plate's ring pattern relative to the mechanical OD of the secondary. The test plate's ring pattern is centered on the optical axis. This measurement shows that the optical axis is within 0.3 mm of the mechanical axis. If the secondary is viewed from the primary when the telescope is horizon-pointing, the displacement of its optical axis is $\Delta x = -0.2 \pm 0.1$ mm, $\Delta y = 0.0 \pm 0.1$ mm.

6. Mechanical dimensions

Apart from a small change in thickness, the mechanical dimensions were set when the mirror was generated by Schott. We did not measure dimensions. The thickness change that occurred during loose-abrasive grinding was less than 0.25 mm.

7. Surface roughness

We measured surface roughness at four locations on the mirror, using a standard procedure. We applied silicone RTV to the surface and allowed it to cure, forming replicas of the surface. We measured the roughness of these replications with a WYKO microscope interferometer. The measured field covers 300×200 microns with a pixel spacing of 0.4 micron. Tilt, focus and astigmatism were removed. The resulting measurement therefore covers spatial frequencies from about 5 to 1000 cycles/mm.

We measured four locations on each 90 mm replication. The measured roughness ranges from 6 to 11 Angstroms rms with an average of 7.5 Angstroms. There is no systematic variation with position on the mirror.

8. References

1. J. H. Burge, "Measurement of large convex aspheres", in *Optical Telescopes of Today and Tomorrow: Following in the Direction of Tycho Brahe*, ed. A. Ardeberg, Proc. SPIE 2871, p. 362 (1997).
2. J. H. Burge, "Error analysis for interferometry with CGH test plates", internal report.